# STUDY ON SNOW COVER CHANGE BASED ON THE FUSION OF SENTINEL-2 AND MODIS IMAGES

Qi Liu[1], Yanli Zhang[1,*]

[1] College of Geography and Environmental Science; Northwest Normal University, Lanzhou, China, liuqinwnu@163.com

**Commission III WG III/9**

**KEY WORDS:** ESTARFM, SNOMAP, Babao River basin, NDSI, Snow Cover Area

**ABSTRACT:**

Snow cover is one of the features that change rapidly on the surface, and remote sensing data with high spatial and temporal resolution is an important means to monitor the dynamic changes of snow. However, due to the limitation of satellite conditions, it is difficult to acquire remote sensing images with both high temporal and spatial resolution at the same time. The classical Enhanced Spatial and Temporal Adaptive Reflectance Fusion Model (ESTARFM) breaks through the limitations of a single sensor and effectively brings into play the complementary advantages of different observation platforms. In this paper, we take the Babao River Basin within the Qinghai-Tibet Plateau as the study area to investigate the effect of fusion of Sentinel-2 and MODIS (Moderate-resolution Imaging Spectroradiometer) based on the ESTARFM and analyze the fusion-supplemented snow accumulation period data. The results show that the fusion effect of Sentinel-2 and MODIS is good in terms of visual and multiple quantitative indicators. The snow accumulation area of the fused image is also close to the real image. By fusing to supplement the missing Sentinel-2 data, a variation map of snow NDSI (Normalized Difference Snow Index) in the study area was obtained. It was found that the snowfall process in the watershed appeared first in the surrounding uplands and then in the flat areas, and the maximum rate of snow cover area change was 116.17 km². Therefore, the spatiotemporal data fusion of Sentinel-2 and MODIS based on ESTARFM algorithm can provide reliable satellite remote sensing data with a higher spatiotemporal resolution for snow accumulation change monitoring.

## 1. INTRODUCTION

As an important component of the cryosphere, snow cover is widely distributed and has significant interannual and seasonal variability. Traditional ground monitoring is difficult to provide full coverage (Zhang et al., 2013). In recent years, remote sensing technology plays an important role in snow cover dynamics monitoring with its advantages of macroscopic, rapid, periodic, multi-scale, multi-level, multi-spectral, and multi-temporal. Since the 1960s, many satellite data have been used for snow remote sensing monitoring (Bai et al., 2013; Wang et al., 2018). Among optical remote sensing, NOAA/AVHRR remote sensing datasets, MODIS snow cover products, Landsat, and other satellite images are commonly used for snow detection. Although MODIS provides snow cover products twice a day, namely MOD10A1 and MOD10Y1, the mixed pixel problem of the 500 m spatial resolution is more prominent, and the snow identification accuracy is generally low, which seriously affects monitoring of the spatial distribution of snow cover (Hall et al., 2002). The Landsat satellite has a long revisit period and is susceptible to the influence of cloud cover, which is not suitable for monitoring and identifying the rapid changes in snow cover (Zhang et al., 2013). Remote sensing images with lower spatial resolution or lower temporal resolution are not conducive to detecting dynamic changes in snow cover and are vulnerable to the influence of cloud cover. Therefore, how to obtain remote sensing images with both high temporal resolution and spatial resolution has become an important issue for monitoring the rapid changes in snow cover (Hall et al., 1995; Hall et al., 2015).

As early as the 1970s, data fusion gradually became a means of data pre-processing for remote sensing applications. In the early days of satellite remote sensing development, data fusion methods mainly focused on coarse resolution multispectral bands by fusing panchromatic bands with high spatial resolution, which can improve the spatial resolution of multispectral images. But this fusion method cannot effectively improve the temporal observation frequency of images. In order to simultaneously improve the temporal and spatial resolutions of satellite images, Gao et al. (2006) proposed a spatial and temporal adaptive reflectance fusion model (STARFM) by taking advantage of the high frequency variation information of surface reflectance provided by MODIS satellite and the detailed surface reflectance provided by the Landsat images. Finally, the daily surface reflectance at Landsat spatial resolution can be produced. However, this method reduces the fusion accuracy in the case of high surface heterogeneity, which is difficult to fuse the surface abrupt changes (Zhuang et al., 2017). Zhu et al. (2010) proposed an enhanced spatial and temporal adaptive reflectance fusion model (ESTARFM), which can improve the fusion accuracy of STARFM in complex heterogeneous surface regions through the trend of reflectance variation between two points in time and the unmixing theory of spectra. The ESTARFM method is simple, and the better fusion effect on heterogeneous regions is one of the fusion algorithms with higher accuracy. Most of the present studies based on Landsat and MODIS data have widely applied this fusion algorithm in the fields of vegetation, crop detection, surface temperature, and lake monitoring (Zhu et al., 2018).

Compared with Landsat, the Multispectral Imager (MSI) on board the Sentinel-2 A/B satellite has a higher temporal resolution (5 days), higher spatial resolution (10 m, 20 m), higher radiometric resolution (12 bit), and spectral resolution (13 spectral bands) (Kääb et al., 2016; Paul et al, 2016; Naegeli et al.,

* Corresponding author
*E-mail address*: zyl0322@nwnu.edu.cn(Y.Zhang).

2017). Zhou et al. (2020) fused Sentinel-2 and MODIS data to establish a vegetation temperature condition index for field drought monitoring; the results showed that high spatial and temporal resolution data fused with MODIS data using Sentinel-2 data had good fusion effects to improve the accuracy of drought monitoring. Snow cover, as one of the fast-changing surfaces, also needs high spatial and temporal resolution data for detection. Therefore, Sentinel-2 has become an important data source for monitoring snow cover changes (Zhang et al., 2020).

In this paper, Taking the Babao River Basin in the upper reaches of the Heihe River Basin in China as the study area, the ESTARFM method is used to fuse MODIS and Sentinel-2 images to monitor the spatiotemporal variation characteristics of snow cover from September 28 to November 27, 2019 by utilizing the fused images with high spatial and temporal resolution.

## 2. STUDY AREA AND DATASETS

### 2.1 Study Area

The Babao River basin is located at the northeastern edge of the Tibetan Plateau (100°06.00′~101°09.05′E, 37°43.01′~38°19.02′). The basin has a total area of about 2452 km², a length of about 105 km, and an elevation of 2709~4678 m. It is the largest tributary of the upper reaches of the Heihe River (Yan et al., 2016). The area has low precipitation, high evaporation, frequent winds and long sunshine hours, and a typical continental alpine mountain climate (He, 2016). The basin is characterized by patchy snow below 3400 m elevation, continuous snow above 3400 m elevation, and perennial snow and permanent glaciers in areas above 4200 m elevation (HiWATER et al., 2012). The Patpong River basin is an ideal basin for snow cover change studies combined with remote sensing.

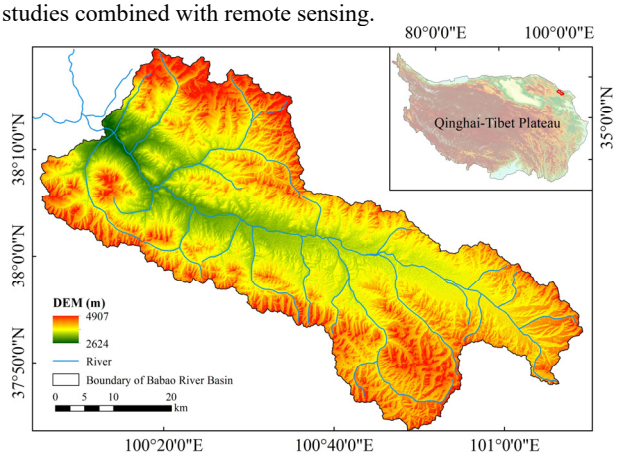


Figure 1. Location of the Babao River Basin

### 2.2 Datasets

In this study, Sentinel-2 and MOD09GA data were selected for fusion experiments. The data in 2020 are used to verify the fusion effect experiment of Sentinel-2 and MOD09GA data; the data in 2019 are used to fuse the missing Sentinel-2 images and study the changes of snow cover in the Babao River basin during the accumulation period. The bands used for the fusion experiment are Green, NIR, and SWIR.1 Sentinel-2 data are from the official website of the European Space Agency (ESA) (https://scihub.copernicus.eu/dhus/#/home), and three images are needed to cover the study area, with orbit number R047 and stitching domain numbers T47SPB, T47SPC & T47SNC. To avoid the effect of cloudiness, images with <5% cloudiness are selected for this study. MOD09GA data are obtained from the official website of NASA (http://ladsweb.nascom.nasa.gov) with 500m spatial resolution, 1d temporal resolution, and orbit number h45v05. According to the requirements of the fusion experiment, the MOD09GA data were reprojected and resampled to generate images with the same scale and 10 m spatial resolution as the UTM-WGS84 projection of Sentinel-2 data. The data acquisition dates are shown in Table 1, the bolded dates are the validation data of the fusion effect, and the rest of the data are the baseline images required for the fusion experiments.

| Sentinel-2 | MOD09GA | Uses of data |
|---|---|---|
| 2020/01/26 | 2020/01/26 | Validate the fusion effect of Sentinel-2 and MOD09GA |
| **2020/01/31** | 2020/01/31 | |
| **2020/02/05** | 2020/02/05 | |
| 2020/02/10 | 2020/02/10 | |
| **2020/02/15** | 2020/02/15 | |
| 2020/02/25 | 2020/02/25 | |
| 2019/09/28<br>2019/10/18<br>2019/10/28<br>2019/11/02<br>2019/11/17<br>2019/11/27 | 2019/09/28-2019/11/27 (61days) | Fusion of Sentinel-2 deficient images to study changes in the snow cover in the study area |

Table 1. Date of Sentinel-2 and MOD09GA data acquisition

## 3. METHODS

The method in this study consists of two main parts, one is the ESTARFM spatiotemporal data fusion method, and the other is the snow extent extraction method. In addition, the workflow of spatiotemporal data fusion and snow cover monitoring is shown in Figure 2.

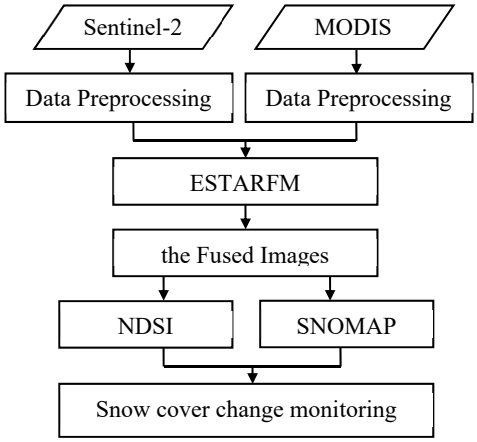


Figure 2. Flow chart of spatiotemporal data fusion and snow cover monitoring

### 3.1 ESTARFM

Zhu et al. (2010) described in detail the principle and use of the ESTARFM data fusion algorithm. This part will further describe ESTARFM's method of integrating Sentinel-2 and MOD09GA on the Babao River Basin. As shown in Fig.3, when the atmospheric correction and error registration are not considered, the ESTARFM method obtains a high-resolution image of the $t_d$ time by establishing a mathematical relationship between the $t_c$ time MOD09GA and Sentinel-2 data with the $t_d$ time MOD09GA data. In the prediction process, the sliding window method is used to reduce the influence of the pixel boundary of low-resolution remote sensing data. When using the sliding window to calculate

the center pixel, the spatial distance, spectral distance and time distance are used as weights. Among them, the prediction algorithm of ESTARFM at $t_c$ and $t_d$ can be described by formula (1):

$$H(x_{\partial/2},y_{\partial/2},t_d,B)=H(x_{\partial/2},y_{\partial/2},t_c,B)+\sum_{i=1}^{n} W_i\times V_i \times(L(x_i,y_i,t_d,B)-L(x_i,y_i,t_c,B)) \quad (1)$$

where $H(x_{\partial/2},y_{\partial/2},t_d,B)$ represents the predicted high resolution pixel value at time $t_d$. $H(x_{\partial/2},y_{\partial/2},t_c,B)$ is the predicted high resolution pixel value at time $t_c$. $(x_{\partial/2},y_{\partial/2})$ is the center pixel of the window. $n$ is the number of similar pixels of the central prediction pixel. $L(x_i,y_i,t_d,B)$ and $L(x_i,y_i,t_c,B)$ are the coarse resolution pixel values at time $t_d$ and $t_c$. $V_i$ is the conversion coefficient of the $i$ similar pixel, and $W_i$ is the weight of the $i$ similar pixel. The prediction algorithm of ESTARFM at $t_d$ and $t_e$ is similar to that at $t_c$ and $t_d$.

Finally, through the weighted sum of the two fusion results, a more accurate Sentinel-2 image at time $t_d$ can be obtained. The weight $\beta_t$ is as shown in formula (2), using $\beta_t$ merges the final $t_d$ time Sentinel-2 image as shown in formula (3) (Zhu et al., 2010). Finally, the real image of Sentinel-2 at time $t_d$ can be used to verify the fusion result.

$$\beta_t=\frac{1/\left|\sum_{j=1}^{\partial}\sum_{i=1}^{\partial}L(x_i,y_j,t_\beta,B)-\sum_{j=1}^{\partial}\sum_{i=1}^{\partial}L(x_i,y_j,t_d,B)\right|}{\sum_{t=c,e}(1/\left|\sum_{j=1}^{\partial}\sum_{i=1}^{\partial}L(x_i,y_j,t_\beta,B)-\sum_{j=1}^{\partial}\sum_{i=1}^{\partial}L(x_i,y_j,t_d,B)\right|)},(t=c,e) \quad (2)$$

$$H(x_{\partial/2},y_{\partial/2},t_d,B)=\beta_c\times H_c(x_{\partial/2},y_{\partial/2},t_d,B)+\beta_e\times H_e(x_{\partial/2},y_{\partial/2},t_d,B) \quad (3)$$

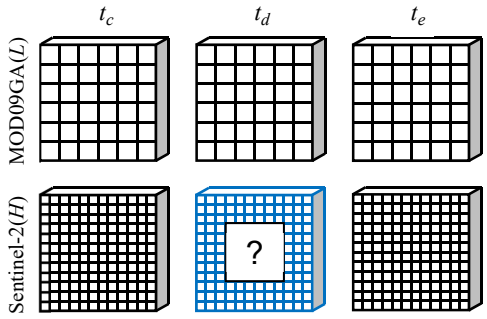


Figure 3. ESTARFM fusion method diagram

### 3.2 Snow area extraction method

This paper uses the SNOMAP algorithm to extract snow extent from Sentinel-2 data and its fusion data. The SNOMAP algorithm is an algorithm proposed by Hall et al. for MODIS snow identification based on the characteristics of snow cover. The normalized differential snow index (NDSI) is the core of the algorithm (Dorothy et al., 1992), based on which the SNOMAP algorithm also adds the near-infrared single-band threshold method discriminant function (NDSI $\geqslant$ 0.4, Band NIR $\geqslant$ 0.11, Band Green $\geqslant$ 0.1) to reduce the risk of clear water, dense vegetation, shaded and low-light conditions the probability of misclassifying the area as snow is reduced. It is also the best technique for snow extraction by optical remote sensing (Yang et al., 2008).

$$NDSI=(Band_{Green}-Band_{SWIR1})/(Band_{Green}+Band_{SWIR1}) \quad (4)$$

## 4. RESULTS

### 4.1 Data fusion accuracy analysis

In this paper, Sentinel-2 and MOD09GA data were fused using ESTARFM method, and the fusion effect was analysed qualitatively and quantitatively. The qualitative analysis was performed from the visual perspective of the fusion effect; the quantitative analysis was performed from the band scatter plot and the statistical map of snow area to analyse the fusion effect of snow extent.

#### 4.1.1 The fusion effect of snow cover pixels

In the paper, fusion images of the study area on January 31, February 5 and February 15, 2020 were obtained by fusion experiments. Figure 4 shows the image of February 15 as an example, and three typical regions of the study area are selected for analysis. Area A is the mountainous area of the watershed, area B is the river area of the watershed, and area C is the flat area of the watershed. The texture details of the fused images of the three regions are extremely close to the real images, and it can be concluded that visually, Sentinel-2 and MOD09GA data have good fusion effect. Similar results are obtained by comparing the results obtained from the fusion of the other two temporal phases.

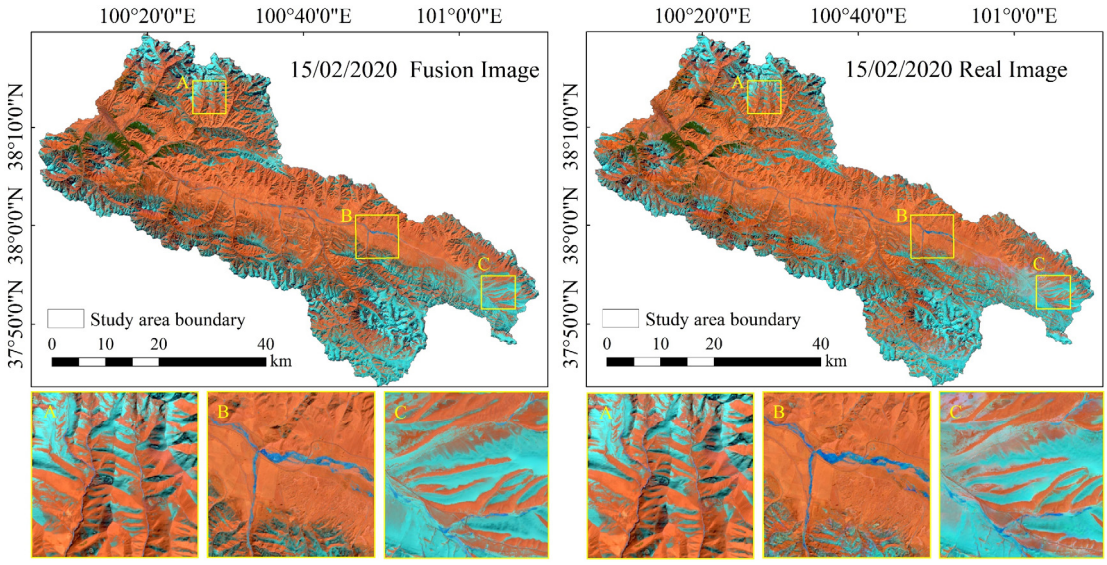


Figure 4. Comparison of fusion results of typical regional data

Figure 5 shows the three bands scatter plots of the generated region C fused image with the corresponding real image at the three times phases mentioned above. The linear equations of the band scatter fit and the coefficient of determination ($R^2$) between the bands are also calculated in the figure. It can be seen in the figure that the scatter points of the nine bands comparison plots are mostly located on both sides of the trend line with concentrated distribution, and the $R^2$ of all bands is above 0.76, which indicates that the reflectance of different bands of the fused image and the original image are highly correlated. Therefore, the image fusion effect obtained by using the ESTARFM algorithm is good.

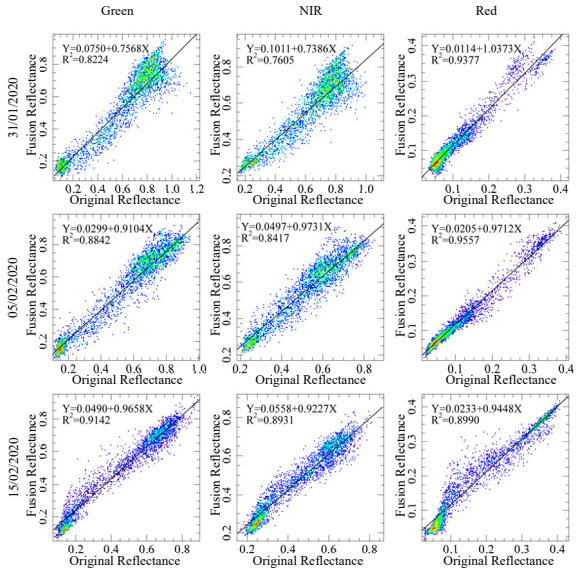


Figure 5. The real and fused images of sentinel- 2 on January 31, February 5 and February 15, 2020 were selected to generate scatter maps in the corresponding Green, NIR, and SWIR1 bands, respectively.

### 4.1.2 Statistical analysis of the data fusion

The previous section concluded that the fusion experiment has a good fusion effect by the comparative analysis of the visual angle and the waveband scatter plot. This section evaluates the fusion effect of images from a qualitative perspective. In this paper, the standard deviation(*std*), information entropy(*ie*), and correlation coefficient(*R*) between the fused image and the real image are calculated for comparison in three-time phases. From Table 2, we can see that the fusion data of all three-time phases have good fusion effect. The standard deviation and information entropy are extremely close to the real images, and the differences are small. The correlation coefficients between the data are all above 0.95, indicating that there is a good correlation between the images. Therefore, the fusion using ESTARFM algorithm has a good fusion effect.

The above experimental procedure focuses on the effect of the data after fusion, but the extent of snow accumulation on the generated data is still unknown. Therefore, in this paper, the snow area of the fused image and the real image under three times phases were extracted using the SNOMAP algorithm, as shown in Table 3, respectively. The table shows that the snow area of the fused image deviates somewhat from the real image, which may be due to the very small amount of clouds on the image input to the ESTARFM model. However, the overall deviation of the snow area between the two seems to be small. Thus, it can be concluded in various quantitative indicators that the snow data generated by fusing Sentinel-2 and MOD09GA data using ESTARFM algorithm works well.

| Date | | Real images | Fused images |
|---|---|---|---|
| 2020/1/31 | *std* | 0.25 | 0.22 |
| 2020/2/5 | | 0.22 | 0.22 |
| 2020/2/15 | | 0.18 | 0.20 |
| 2020/1/31 | *ie* | 0.4408 | 0.4401 |
| 2020/2/5 | | 0.4405 | 0.4401 |
| 2020/2/15 | | 0.4402 | 0.4399 |
| 2020/1/31 | *R* | 0.96 | |
| 2020/2/5 | | 0.97 | |
| 2020/2/15 | | 0.97 | |

Table 2. Statistical table of data fusion results

| Date | Snow cover area (km²) | |
|---|---|---|
| | Fusion Images | Real Images |
| 2020/1/31 | 907.48 | 923.36 |
| 2020/2/5 | 858.66 | 885.72 |
| 2020/2/15 | 715.41 | 726.12 |

Table 3. Comparison of snow cover area between fused image and real image

### 4.2 Sentinel-2 fused with MODIS data to monitor snow cover changes

It is well known that the revisit period of Sentinel-2 data is 5days. but due to the influence of cloudy and rainy weather, optical data such as Sentinel-2 are difficult to be acquired continuously for a long time, which hinders the study of monitoring snow changes to some extent. Through the fusion experiments in Section 4.1, it can be understood that the desired or Sentinel-2 missing images can be acquired using the spatiotemporal data fusion method with a good fusion effect. Therefore, in this paper, based on the ESTARFM algorithm, we fused Sentinel-2 and MOD09GA data (as in Table 1) to generate daily high-resolution snow images from September 28 to November 27, 2019 in the Babao River basin, which improved the ability of optical data to monitor snow cover changes.

The NDSI is an important index for monitoring snowpack change monitoring. Only the snow extent of the data can be extracted using the SNOMAP algorithm. Therefore, the snow extent of the fused image and Sentinel-2 data was extracted using the SNOMAP algorithm, and the NDSI value corresponding to it was extracted using the snow extent to obtain the image shown in Figure 5. The process of the NDSI of the snow accumulation during the rapid accumulation period from September 28 to November 27, 2019, can be clearly seen in the figure. Of course, by reviewing the historical weather in the county where the study area is located, there is a similar snowfall process (Fig. 7). Combining Fig. 6 and Fig. 7, we can get that the Babao River basin, which belongs to the northeastern edge of the Tibetan Plateau, began to cool down in early October, and snow gradually started to fall in the higher elevation mountainous areas. And because the surface was not covered with snow before, after a snowfall, the surface of the surrounding uplands began to be covered with snow, and the NDSI value would change a lot. In the middle and second half of October, the rainfall decreased and the temperature recovered, but the overall temperature was not high; the snow cover area (SCA) of the surrounding uplands in the study area decreased, but not much. In November, the

temperature in the study area continued to be low, but there were some fluctuations; after at the end of November, the weather improved and the temperature slightly recovered, and the snow area decreased accordingly, and the lower the elevation, the faster the snow melted. The fastest growth rate of snow area by calculation occurred from November 2 to November 7, with a growth rate of 116.2km²/days.

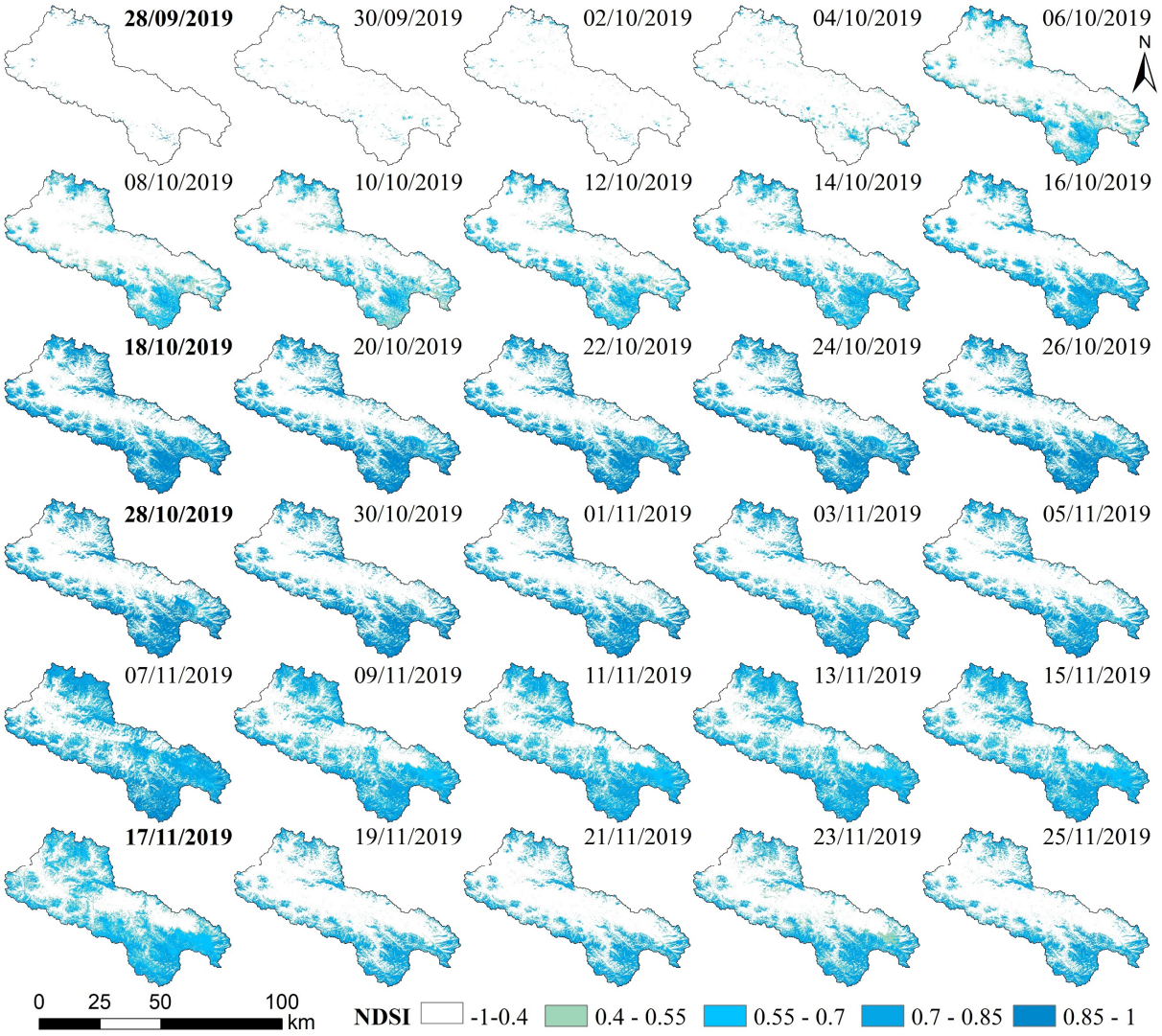


Figure 6. Temporal and spatial variation of snow cover on alternate days from September 28 to November 27, 2019

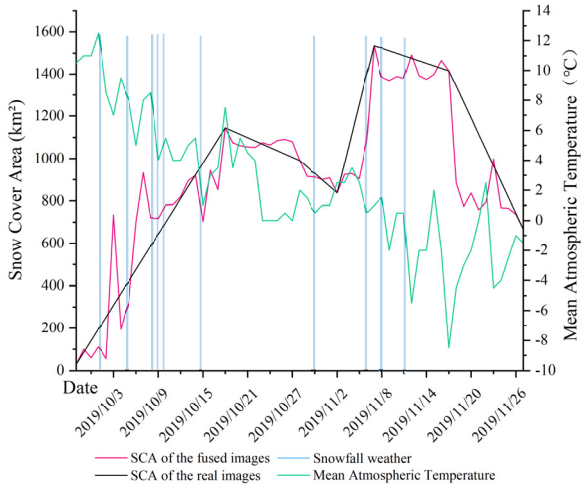


Figure 7. The relationship between the snow cover area and weather changes of Sentinel-2 data and fusion data

Throughout the accumulation period, we can see that only 6 times phases of Sentinel-2 data can participate in the fusion operation due to the weather conditions and cloud cover. It is clear from the above fusion experiments that the fusion of images with missing time phases using ESTARFM algorithm can make up the required data. The spatial variation of snow area and the process of area change are studied from the sky scale.

## 5. CONCLUSIONS AND DISCUSSION

In this paper, the ESTARFM algorithm was applied to the fusion of Sentinel-2 and MODIS data to obtain the fused images of January 31, February 5 and February 15, 2020 in the Babao River basin, and the qualitative and quantitative analysis and evaluation of the fusion results were carried out using the Sentinel-2 real images of the corresponding dates. The experimental results showed that there was no significant difference between the fused images of the three-time phases and the corresponding real images by visual comparison of the image fusion effect in the same area. The scatter plots of the three bands corresponding to the fused image and the real image have good symmetry; the

This contribution has been peer-reviewed. The double-blind peer-review was conducted on the basis of the full paper.
https://doi.org/10.5194/isprs-annals-V-3-2022-333-2022 | © Author(s) 2022. CC BY 4.0 License.

fused image has high separability and the amount of information carried is close to that of the real image. The snow area of the fused image and the real image are extracted with the same snow extraction method, and the area difference is not significant. In summary, the snow image generated by fusing Sentinel-2 and MODIS data using ESTARFM algorithm has a good fusion effect.

In order to monitor the rapid changes of snow accumulation, the Sentinel-2 images that were missing due to the influence of clouds and rain in the 2019 snow accumulation period from September 28 to November 27 in the study area were fused and supplemented based on the better quality Sentinel-2 images fused with MODIS data, resulting in 55 time-phase high-resolution fused images of snow accumulation from September to November. The spatiotemporal data fusion method greatly improves the efficiency of Sentinel-2 image use and facilitates the monitoring of snow dynamics compared to the available 6 time-phases of images collected without fusion. In this paper, the data fusion method is used to reconstruct the poor quality Sentinel-2 data with a temporal resolution of 1d, thus providing a high-quality remote sensing data source for monitoring rapid surface changes such as long time series snow accumulation.

This study proposes the use of a spatiotemporal data fusion model to obtain daily high-resolution remote sensing data of the Baba River basin, which to some extent alleviates the problem of missing data due to the limitation of the data itself and is important for future studies on snow monitoring in small-scale areas. However, the influence of meteorological factors was not considered in the fusion process of the model in this study. Therefore, the consideration of meteorological conditions can be added to future snow cover change monitoring studies to further improve the accuracy of snow cover monitoring data generated using spatiotemporal data models.

## ACKNOWLEDGEMENTS

This research was supported by the National Natural Science Foundation of China (NSFC) project, grant number 41871277 and number 41561080, and the China Postdoctoral Fund project grant number 2016M602893. The authors would like to thank ESA (European Space Agency) and NASA (National Aeronautics and Space Administration) for the data provided.

## REFERENCES

Yu LX, Zhang SW, Bu K, et al. A Review on Snow Data Sets[J]. *Scientia Geographica Sinica*, 2013, 33(07):878-883.

Bai YC, Feng XZ. Introduction to Some Research Work on Snow Remote Sensing[J]. *Remote Sensing Technology and Application*, 1997(02):60-66.

Wang J, Che T, Li Z, et al. Investigation on Snow Characteristics and Their Distribution in China[J]. *Advances in Earth Science*, 2018, 33(01):12-26.

Dorothy K Hall,George A Riggs,Vincent V Salomonson,Nicolo E DiGirolamo,Klaus J Bayr. MODIS snow-cover products[J]. *Remote Sensing of Environment*, 2002, 83(1).

Hall D K, Salomonson V V, Riggs G A. Development of methods for mapping global snow cover using moderate resolution imaging spectroradiometer data[J]. *Remote Sensing of Environment*, 1995, 54(2).

Hall D K, Crawford C J, Digirolamo N E, et al. Detection of earlier snowmelt in the Wind River Range, Wyoming, using Landsat imagery, 1972–2013[J]. *Remote Sensing of Environment*, 2015, 162:45-54.

Zhuang XY. A Spatial-Temporal Data Fusion Method Based on Landsat 8 OLI and MODIS data[D]. Nanjing University,2017.

Gao F, Masek J, Schwaller M, et al. On the blending of the Landsat and MODIS surface reflectance: Predicting daily Landsat surface reflectance[J]. *IEEE Transactions on Geoscience and Remote sensing*, 2006, 44(8): 2207-2218.

Xiaolin Zhu,Jin Chen,Feng Gao,Xuehong Chen,Jeffrey G. Masek. An enhanced spatial and temporal adaptive reflectance fusion model for complex heterogeneous regions[J]. *Remote Sensing of Environment*, 2010, 114(11).

Zhu X, Cai F, Tian J, et al. Spatiotemporal Fusion of Multisource Remote Sensing Data: Literature Survey, Taxonomy, Principles, Applications, and Future Directions[J]. *Remote Sensing*, 2018, 10(4):527-.

Zhou X, Wang P, Tansey K, et al. Developing a fused vegetation temperature condition index for drought monitoring at field scales using Sentinel-2 and MODIS imagery[J]. *Computers and Electronics in Agriculture*, 2020, 168:105144.

Kääb A, Winsvold S H, Altena B, et al. Glacier remote sensing using Sentinel-2. part I: Radiometric and geometric performance, and application to ice velocity[J]. *Remote Sensing*, 2016, 8(7): 598.

Paul F, Winsvold S H, Kääb A, et al. Glacier remote sensing using Sentinel-2. Part II: Mapping glacier extents and surface facies, and comparison to Landsat 8[J]. *Remote Sensing*, 2016, 8(7): 575.

Naegeli K, Damm A, Huss M, et al. Cross-Comparison of Sentinel-2 and Landsat 8 Albedo Products for Glacier Surfaces[C]//AGU Fall Meeting Abstracts. 2016, 2016: C13D-0864.

Yan Y N, Che T, Li H Y, et al. Using snow remote sensing data to improve the simulation accuracy of spring snowmelt runoff: take Babao River basin as an example[J]. *Journal of Glaciology and Geocryology*, 2016, 38(1):211-221.

He Y Q. Snow Hydrological Simulation in Alpine Areas using Remote Sensing and GIS Technologies[D]. Lanzhou University, 2014.

HiWATER:An Integrated Remote Sensing Experiment on Hydrological and Ecological Processes in the Heihe River Basin[J]. *Advances in Earth Science*, 2012, 27(5): 481-498.

Yang X C, Cao Y G, Bin X U, et al. Remote sensing monitoring of grassland snow in China: From October 2007 to March 2008[J]. *Geographical Research*, 2008, 27(5):1109-1117.

Zhang Y L, Zhang L P. Snow cover identification and area Change in mountainous regions on Sentinel-2 time series Data[J]. *Chinese Journal of Ecology*, 2020, 39(08): 2810-2820.